Supporting information

Highly rapid and non-enzymatic detection of cholesterol based on carbon nitride quantum dots as fluorescent nanoprobes

Ying Chen, Gege Yang, Shanshan Gao, Liangliang Zhang, Mengdi Yu, Chunxia Song*, Ying Lu*

Department of Applied Chemistry, School of Science, Anhui Agricultural University, Hefei 230036, China

*Corresponding author

E-mail: songchunxia@ahau.edu.cn (C. Song), luy@ahau.edu.cn (Y. Lu).

1. FTIR spectrum of CNQDs

2. XPS result of CNQDs

3. The optical properties of the CNQDs

4. The fluorescence emission spectra of CNQDs under different excitation wavelength

5. Measurement of the quantum yield

6. Comparison of the analytical performance with the reported cholesterol detection methods

7. Determination of cholesterol in fetal bovine serum

1. FTIR spectrum of CNQDs.

FTIR was used to characterize the organic group of the obtained CNQDs. As shown in Fig. S1, the sharp absorption peak at 802 cm^{-1} attributed to the characteristic breathing mode of tri-s-triazine units.[1] The peaks range from 1300 to 1660 cm^{-1} represented the stretching modes of CN heterocycles. The peaks between 3000 and 3400 cm^{-1} could be assigned to N-H and O-H stretching adsorptions, indicating the presence of -NH and -NH$_2$.[2]
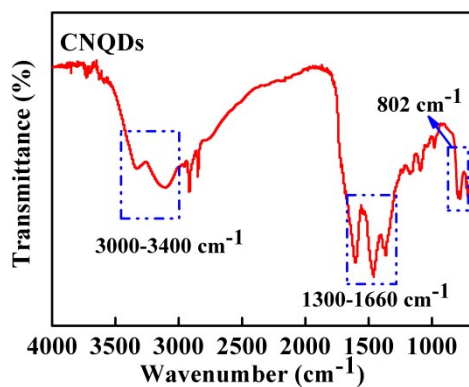

Fig. S1 FTIR spectrum of the CNQDs

2. XPS result of CNQDs

To disclose the chemical composition and states of the CNQDs, XPS measurement was conducted. As shown in Fig. S2A, the wide-scan XPS spectrum of CNQDs unraveled three primarily elemental peaks due to the C, N, and O, respectively. The high resolution C 1s spectrum (Fig. S2B) could be resolved into four peaks with binding energies (BEs) at 284.8, 286.3, 287.8, and 289.1 eV, corresponding to bonds of the C-C, C-O, N-C=N, and O-C=O, respectively. The N 1s spectrum (Fig. S2C) exhibited three main peaks at 398.6, 399.8, and 400.1 eV attributable to C=N-C, C-N-C, and N-(C)$_3$, respectively. The high resolution O 1s spectrum (Fig. S2D) could be fitted into two peaks centered at 531.9 and 532.4 eV, assigning to the C-OH/C-O-C and C=O bonds, respectively.[3, 4]
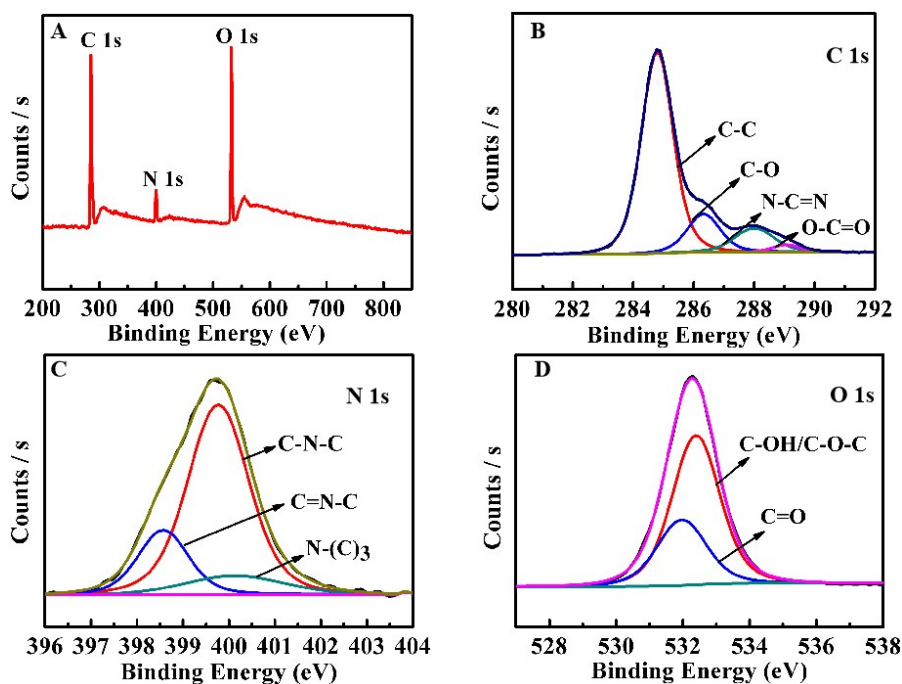

Fig. S2 (A) XPS survey spectrum of CNQDs; (B) High-resolution peak-fitted XPS of the C 1s regions of CNQDs; (C) High-resolution peak-fitted XPS of the N 1s regions of CNQDs; (D) High-resolution peak-fitted XPS of the O 1s regions of CNQDs.

3. The optical properties of the CNQDs

The UV-vis absorption spectrum and the fluorescence spectra of the CNQDs were shown in Fig. S3A, the fluorescence emission peaks of CNQDs and bulk g-C$_3$N$_4$ were measured and displayed in Fig. S3B.
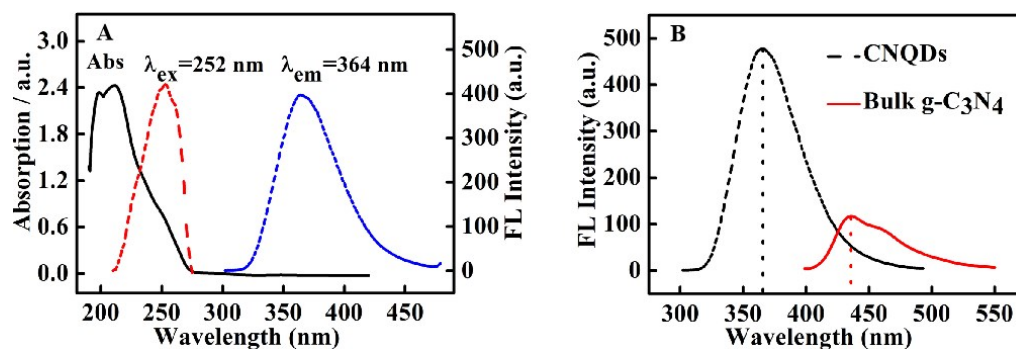

Fig. S3 (A) The UV-vis absorption spectrum (Abs, black curves), fluorescence excitation spectrum (λ_{ex}=252 nm, red curve) and the fluorescence emission spectrum (λ_{em}=364 nm, blue curve) of CNQDs; (B) The fluorescence emission spectra of CNQDs (black curve) and bulk g-C$_3$N$_4$ (red curve).

4. The fluorescence emission spectra of CNQDs under different excitation wavelength

The fluorescence emission spectra of CNQDs under different excitation wavelength was measured and shown in Fig. S4A, the excitation wavelength was changed by the 10 nm increments within the range of 210-280 nm. The relationship of the fluorescence intensity versus the excitation wavelength was shown in Fig. S4B, the excitation wavelength at 250 nm was selected as the fluorescence excitation wavelength of the system.
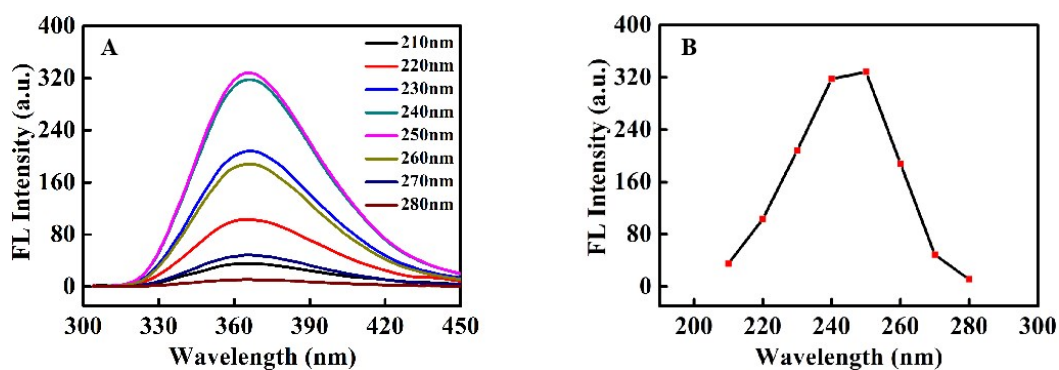

Fig. S4 (A) The fluorescence emission spectra of CNQDs under different excitation wavelength ranging from 210 to 280 nm; (B) Relationship between the fluorescence intensity of CNQDs and the excitation wavelength. The excitation/emission slits were 2.5 nm and 5 nm, respectively.

5. Measurement of the quantum yield

In this work, the fluorescence quantum yield of CNQDs was measured by using the reported method.[5] The quantum yield of L-tyrosine was 0.14 at the excitation wavelength of 275 nm.[6] In order to reduce the inner filter effect, the concentration of L-tyrosine and CNQDs was diluted to less than 0.05 of the absorbance. The quantum yield of CNQDs was calculated by the following formula.

$$\Phi_s = \Phi_r \times (\int I_s / \int I_r) \times (A_r / A_s) \times (n_s / n_r)^2$$

Here, "s" and "r" represented the CNQDs and L-tyrosine, respectively; Φ was the fluorescence quantum yield, $\int I$ denoted the measured fluorescence integrated area; A was the absorbance at the excitation wavelength (the excitation wavelength of CNQDs at 250 nm and L-tyrosine at 275 nm), and n represented the refractive index of the solvent.

Tab. S1 Fluorescence quantum yield of the CNQDs by using L-tyrosine as a standard solution.

Sample	Fluorescence integrated area	Absorbance	Fefractive index of solvent	Quantum yield
L-tyrosine	1580.56538	0.044	1.333	0.14
CNQDs	3313.86505	0.037	1.333	0.35

6. Comparison of the analytical performance with the reported cholesterol detection methods

Tab. S2 Comparison of the analytical performance with the reported cholesterol detection methods.

Materials	Method	Linear range	Detection limit	References
Nafion/[a]Bi-Pt	CV	0.05- 22 mM	50 μM	[7]
[b]AgNPs	CV	0.28–3.3 mM	180 μM	[8]
poly(luminol-biotinylated pyrrole)	ECL	15–800 μM	14.7 μM	[9]
[c]Pt/rGO/P3ABA	CV	0.25–4.00 mM	40.5 μM	[10]
[d]MEAB	CV	1–12 mM	440 μM	[11]
CNQDs	fluorescence	0-500 μM	10.93 μM	This work

[a]Bi-Pt: Bi (bismuth) adatoms modified Pt (platinum); [b]AgNPs: silver nanoparticles; [c]Pt/rGO/P3ABA: platinum/reduced graphene oxide/poly (3-aminobenzoic acid); [d]MEAB: microneedle electrode array-based biosensor.

7. Determination of cholesterol in fetal bovine serum

Tab. S3 Detection of cholesterol in fetal bovine serum (n=3).

Sample	Added (μM)	Founded (μM)	Recovery (%)	RSD (%)
1	10.00	10.08±0.35	100.8	3.5
2	50.00	47.51±2.16	95.0	4.6
3	100.00	105.60±2.53	105.6	2.4
4	250.00	245.73±5.07	98.3	2.1
5	500.00	516.17±11.34	103.2	2.2

References

S1.   X. Guo, Y. Wang, F. Wu, Y. Ni and S. Kokot, *Microchim. Acta*, 2015, **183**, 773-780.

S2.   X. Zhang, X. Xie, H. Wang, J. Zhang, B. Pan and Y. Xie, *J. Am. Chem. Soc.*, 2013, **135**, 18-21.

S3.   J. Zhou, Y. Yang and C. Zhang, *Chem. Commun.*, 2013, **49**, 8605-8607.

S4.   Z. Song, T. Lin, L. Lin, S. Lin, F. Fu, X. Wang and L. Guo, *Angew. Chem. Int. Ed.*, 2016, **55**, 2773-2777.

S5.   A. Antaris, H. Chen, S. Diao, Z. Ma, Z. Zhang, S. Zhu, J. Wang, A. Lozano, Q. Fan, L. Chew, M. Zhu, K. Cheng, X. Hong, H. Dai and Z. Cheng, *Nat. Commun.*, 2017, **8**, 15269.

S6.   Y. Li, J. Cai, F. Liu, H. Yu, F. Lin, H. Yang, Y. Lin and S. Li, *Microchim. Acta*, 2018, **185**, 134.

S7.   V. Soorya and S. Berchmans, *Mater. Sci. Eng., C*, 2016, **64**, 183-189.

S8.   Y. Li, H. Bai, Q. Liu, J. Bao, M. Han and Z. Dai, *Biosens. Bioelectron.*, 2010, **25**, 2356-2360.

S9.   B. Claver, A. Cabello, M. Sanfrutos, M. Fernandez, V. Miron, S. Gonzalez and C. Vallvey, *Anal. Chim. Acta*, 2012, **754**, 91-98.

S10.   S. Phetsang, J. Jakmunee, P. Mungkornasawakul, R. Laocharoensuk and K. Ounnunkad, *Bioelectrochem.*, 2019, **127**, 125-135.

S11.   J. Gao, W. Huang, Z. Chen, C. Yi and L. Jiang, *Sens. Actuators, B*, 2019, **287**, 102-110.